



A new high-pressure benzocaine polymorph — towards understanding the molecular aggregation in crystals of an important active pharmaceutical ingredient (API)

Ewa Patyk-Kaźmierczak* and Michał Kaźmierczak*

Received 20 September 2019

Accepted 8 December 2019

Edited by J. Lipkowski, Polish Academy of Sciences, Poland

Keywords: benzocaine; high-pressure polymorphism; data-mining; hydrogen bonds.**CCDC references:** 1949574; 1949575; 1949576; 1949577; 1949578; 1949579; 1949580; 1949581**Supporting information:** this article has supporting information at journals.iucr.org/b

Faculty of Chemistry, Adam Mickiewicz University in Poznań, Uniwersytetu Poznańskiego 8, Poznań, 61-614, Poland.

*Correspondence e-mail: ewapatyk@amu.edu.pl, kax@amu.edu.pl

Benzocaine (BZC), an efficient and highly permeable anaesthetic and an active pharmaceutical ingredient of many commercially available drugs, was studied under high pressure up to 0.78 GPa. As a result, new BZC polymorph (IV) was discovered. The crystallization of polymorph (IV) can be initiated by heating crystals of polymorph (I) at a pressure of at least 0.45 GPa or by their compression to 0.60 GPa. However, no phase transition from polymorph (I) to (IV) was observed. Although polymorph (IV) exhibits the same main aggregation motif as in previously reported BZC polymorphs (I)–(III), *i.e.* a hydrogen-bonded ribbon, its molecular packing and hydrogen-bonding pattern differ considerably. The N–H···N hydrogen bonds joining parallel BZC ribbons in crystals at ambient pressure are eliminated in polymorph (IV), and BZC ribbons become positioned at an angle of about 80°. Unfortunately, crystals of polymorph (IV) were not preserved on pressure release, and depending on the decompression protocol they transformed into polymorph (II) or (I).

1. Introduction

Benzocaine (BZC), 4-aminobenzoic acid ethyl ester, is a local anaesthetic almost exclusively administered topically. Its pain-relief action is associated with BZC molecules binding to the phenylalanine residue in Na⁺ neuron channels *via* N–H··· π and π ··· π interactions, preventing the transmission of impulses at nerve endings and along nerve fibres (Butterworth & Strichartz, 1990; Hanck *et al.*, 2009; Aguado *et al.*, 2013). BZC is an active pharmaceutical ingredient (API) of 583 over-the-counter drugs, commercially available in the USA and Canada, in the form of gels (402), liquids (63), swabs (25), creams (20), ointments (15), sprays (15), *etc.* (Law *et al.*, 2014). It belongs to class II of the Biopharmaceutical Classification System (Amidon *et al.*, 1995; Mehta, 2017) and as such has high permeability ($1.11 \times 10^{-4} \text{ cm s}^{-1}$; Juni *et al.*, 1977) and low water solubility (0.131 mg ml^{-1} in 30°C; Bottari *et al.*, 1977). Therefore, in a similar way to other bioactive compounds from class II, BZC bioavailability is limited by its solubility.

The solubility of all compounds strongly depends on the hydrogen-bonding pattern formed in a solid state. Therefore, analysis of intermolecular interactions present in solid forms of APIs is an important aspect of drug development (Gao *et al.*, 2017). Such insight not only enables a better understanding of the physicochemical properties of APIs, but also provides information about the hierarchy of supramolecular synthons,

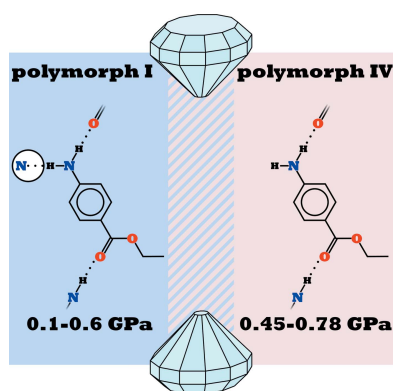


Table 1
Crystallographic data for BZC polymorphs.

For full version of the table please refer to Table S1.

Phase	(I)	(II) [†]	(III) [†]	(IV)
<i>T</i> (K)	298	300	150	298
<i>p</i> (GPa)	0.10	0.0001	0.0001	0.55
Crystal system	Monoclinic	Orthorhombic	Monoclinic	Monoclinic
Space group	<i>P2₁/c</i>	<i>P2₁2₁2₁</i>	<i>P112₁</i>	<i>P2₁/c</i>
<i>a</i> , <i>b</i> , <i>c</i> (Å)	8.193 (1), 5.454 (1), 20.07 (5)	8.2424 (4), 5.3111 (3), 20.904 (1)	8.1883 (4), 10.640 (1), 20.476 (1)	6.305 (1), 5.1839 (4), 24.94 (8)
α , β , γ (°)	90, 91.47 (4), 90	90, 90, 90	90, 90, 99.370 (2)	90, 96.25 (8), 90
Unit-cell volume (Å ³)	896 (2)	915.12 (9)	1760.05 (15)	810 (3)
<i>Z</i> , <i>Z'</i>	4, 1	4, 1	8, 4	4, 1
<i>D_x</i> (g cm ⁻³)	1.224	1.199	1.247	1.354
<i>R</i> ₁ , <i>wR</i> ₂ [<i>I</i> > 4σ(<i>I</i>)], GooF	0.0610, 0.1485, 1.000	0.0392, 0.1035, 1.059	0.065, 0.091, 2.103	0.0910, 0.2073, 1.157

[†] Crystallographic data cited after Chan *et al.* (2009), structure refcodes: polymorph (II)-QQQAXG05; polymorph (III)-QQQAXG03.

which is essential for the design of novel cocrystals of biologically active compounds (Bis *et al.*, 2007; Shattock *et al.*, 2008; Cheney *et al.*, 2010; Bučar *et al.*, 2014). This crystal engineering approach to the modification of intermolecular interactions by incorporation of cofomer molecules allows for the fine-tuning of the properties of the final drug product, such as solubility (Smith *et al.*, 2011; Geng *et al.*, 2013) and stability (Gadade & Pekamwar, 2016). Even slight changes in the hydrogen-bonding pattern supporting the crystal structure, as observed between polymorphs, can result in varied properties of different solid forms of the same compound (Braga *et al.*, 2009). In fact, it was recently reported that polymorphs (I)–(III) of BZC differ in solubility and permeability (Paczkowska *et al.*, 2018). Until now three polymorphs of BZC were known. At ambient conditions, BZC exists in two forms: monoclinic polymorph (I) (space group *P2₁/c*, Lynch & McClenaghan, 2002) and orthorhombic polymorph (II) (space group *P2₁2₁2₁*; Sinha & Pattabhi, 1987). On cooling to 150 K, polymorph (II) undergoes a solid-to-solid phase transition to polymorph (III) of monoclinic symmetry, space group *P112₁* (Chan *et al.*, 2009). Depending on the milling protocol, polymorph (III) can transform to polymorph (I) (ball milling) or polymorph (II) (micro milling; Paczkowska *et al.*, 2018). In all reported forms of BZC, molecules are hydrogen-bonded *via* N–H...O hydrogen bonds into ribbons, and a similar positioning of so-formed ribbons in respect to each other is observed.

Investigation of polymorphism is an important stage of drug development. It provides information on the stability of the solid forms of the API that can affect the properties of the final product (Lee, 2014). It is also an important legal matter, as each polymorph is considered a new material by the US Food and Drug Administration (FDA, 2007) and as such a patent-eligible subject matter. However, the search for polymorphs is often limited to varied-temperature conditions at ambient pressure and modification of solvent systems. Meanwhile, the application of high pressure for polymorph screening can significantly broaden the spectrum of experimental conditions, leading to the discovery of new crystal forms (Fabbiani *et al.*, 2004, 2007; Fabbiani & Pulham, 2006; Boldyreva, 2007, 2016; Johnstone *et al.*, 2010; Patyk & Katrusiak, 2015; Patyk *et al.*, 2015*a,b*, 2016; Marciniak *et al.*,

2016*a,b*; Zakharov *et al.*, 2016; Zakharov & Boldyreva, 2019). Previous research showed that pressure can provide a sufficiently strong stimulus to enforce phase transitions in compounds considered to exist only in one crystal form (*e.g.* sucrose; Patyk *et al.*, 2012), or to allow access to theoretically predicted metastable phases (Neumann *et al.*, 2015). In this work, a study of high-pressure polymorphism of BZC is presented and its new polymorph (IV) is introduced. Results are complemented with analysis and comparison of the crystal structure of polymorph (IV) with the three previously reported crystal forms.

2. Experimental

2.1. High-pressure crystallization and X-ray measurements

In all experiments, as-received benzocaine from Sigma-Aldrich was used. The powder X-ray diffraction (PXRD) confirmed that the received sample was a mixture of polymorphs (I) and (II) (Fig. S1). A small number of crystals of BZC, alongside small ruby chip, were loaded into an opening (0.4–0.5 mm diameter) in steel gasket (0.3 mm thick) mounted in modified Merrill–Bassett diamond anvil cell (DAC; Merrill & Bassett, 1974). For the experiments two types of BZC-saturated hydrostatic medium were used: 97.5% DMSO solution in water and MeOH:EtOH:H₂O mixture (16:3:1 volume). After loading, the pressure inside the DAC was gradually increased up to 0.78 GPa. The sample was recrystallized *in situ* (Figs. S3–S6, S8–S10) at each step before X-ray diffraction measurement (except for the measurement at 0.65 GPa, where the sample was obtained after releasing pressure from 0.78 GPa, Fig. S7). The pressure inside the DAC was measured by the ruby fluorescence method (Piermarini *et al.*, 1975) with a Photon Control Inc. spectrometer affording a 0.02 GPa accuracy. Two series of experiments in the different hydrostatic medium were performed: (i) when DMSO was used as hydrostatic medium, crystals were grown and measured at 0.22 (2), 0.41 (2), 0.50 (2), 0.52 (2) GPa (the measurement at 0.22 GPa was used only for unit-cell parameters measurement due to the insufficient quality of the collected data), and (ii) when MeOH:EtOH:H₂O was used at

0.10 (2), 0.30 (2), 0.55 (2), 0.65 (2) and 0.78 (2) GPa. The X-ray diffraction experiments were performed with Mo $K\alpha$ graphite-monochromated radiation and the four-circle Xcalibur diffractometer equipped in the EOS CCD detector. The *CrysAlis PRO* software (2015) was used for data collection, determination of the *UB*-matrix, absorption corrections and data reduction. The crystal structures were solved by intrinsic phasing with *SHELXT* (Sheldrick, 2015a) and refined by least-squares with program *SHELXL* (Sheldrick, 2015b). The positions of hydrogen atoms were determined based on hybridization of carrier atoms with U_{iso} equal to $1.2U_{\text{eq}}$ for aromatic and secondary C carriers, as well as N carriers, and equal to $1.5U_{\text{eq}}$ for primary C carriers. The length of N–H and C–hydrogen bonds was fixed to the distances of 0.93 Å for aromatic carbon atoms, 0.96 or 0.97 Å for primary and secondary carbon atoms, respectively, and 0.87 Å for nitrogen atoms. All crystal structures have been deposited with the Cambridge Crystallographic Data Centre (Groom *et al.*, 2016; CCDC Nos. 1949574–1949581). Copies of the data can be accessed, free of charge, by filling online the application form at <https://www.ccdc.cam.ac.uk/structures/>. Selected crystallographic data for polymorphs (I) and (IV) at 0.10 and 0.55 GPa, respectively, alongside data for polymorphs (II) and (III), are listed in Table 1. Detailed crystallographic data for BZC polymorphs are presented in the supporting information (Table S1).

In order to establish pressure limits for the crystallization of BZC polymorphs, a visual observation of its crystal compressed in the DAC was performed (Figs. S11 and S12). The pressure of 0.60 (2) GPa was the lowest at which initiation of the crystallization was observed (Fig. S12, Movie S1). During the growth of the new crystal, the dissolution of primary crystal was observed. The recrystallization was completed at pressure of 0.48 (2) GPa and the single-crystal X-ray diffraction (SCXRD) method was used to determine the lattice parameters.

Stability of new BZC polymorph was investigated by visual observation, on the pressure release at various rates: (i) slowly, followed by 40-days delay in DAC opening (Figs. S13 and S14); (ii) rapidly, followed by immediate DAC opening. In both cases, recovered samples were studied *via* SCXRD and/or PXRD techniques (Fig. S2).

2.2. Structural analysis

The Cambridge Structural Database (CSD version 5.40; May 2019; Groom *et al.*, 2016) and DrugBank (version 5.1.3; April, 2nd 2019; Law *et al.*, 2014) has been data-mined for structures of esters of *p*-aminobenzoic acid (PABA) and its derivatives using *ConQuest* (Bruno *et al.*, 2002) and CSD Python API (here: Application Programming Interface). The following restrictions have been used for the CSD survey: (i) 3D coordinates determined; (ii) one chemical unit in the entry; (iii) disordered, ionic and metal–organic structures have been excluded. Search in the DrugBank was limited to entries marked as approved. In both cases of data mining, compounds containing nitrile, hydroxyl, aldehyde, and carbonyl (except

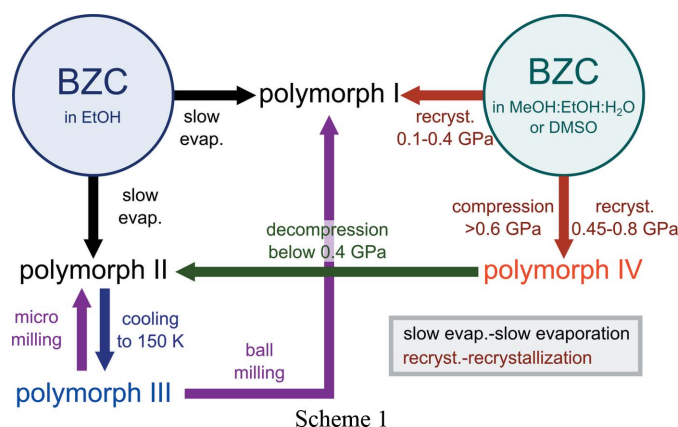
ester) groups were omitted. Moreover, depositions with more than one ester or primary amine group, or lactone ring were excluded from statistical analysis. Additionally, the CSD has been surveyed for primary amine–ester synthons.

The *D*–*H*···*A* intermolecular hydrogen bonds were assigned using following criteria: (i) the distance between hydrogen and acceptor atoms must be smaller than the sum of van der Waals radii of involved atoms (Bondi, 1964); (ii) hydrogen atoms must be directed towards acceptor atoms.

Enthalpies of formation were calculated for crystals of polymorphs (I) and (IV) (in the whole investigated pressure range) using *MOPAC2016:Hamiltonian PM7* (Stewart, 2016).

3. Results and discussion

We have shown that during recrystallization under the pressure of up to 0.41 GPa, polymorph (I) is a preferred form of BZC. Even if BZC crystals were dissolved entirely, on cooling, the crystals of polymorph (I) emerged. Above 0.45 GPa, on recrystallization *via* heating and subsequent cooling, BZC crystallizes in a new form, polymorph (IV), of monoclinic symmetry, space group $P2_1/c$, and it exists up to 0.78 GPa at least. Polymorph (IV) can be also obtained isothermally by increasing pressure to 0.60 GPa. Above this pressure, polymorph (I) crystals gradually dissolve and growth of polymorph (IV) crystals can be observed (Movie S1). After completion of the crystallization, the pressure was stabilized at 0.48 GPa, and polymorph (IV) crystals remained stable. Only when pressure is released, crystals of polymorph (IV) undergo a destructive phase transition to polymorph (II), observed visually and confirmed by PXRD measurement of the sample immediately recovered from the DAC (Fig. S2). Interestingly, when pressure was released slowly to 0.2 GPa and left for 40 days, recrystallization of sample to polymorph (I) occurred. The current state of knowledge on the relationship between four BZC polymorphs was mapped in Scheme 1. Methods for ambient-pressure crystallization of polymorphs (I)–(III) are cited after previous reports (Sinha & Pattabhi, 1987; Lynch & McClenaghan, 2002; Chan *et al.*, 2009; Paczkowska *et al.*, 2018).



Although newly obtained polymorph (IV) crystallizes in the same space group as polymorph (I), the behaviour of their crystals on compression differ. The unit-cell volume of poly-

morph (I) decreases of 46 \AA^3 (approx. 5% of the ambient-conditions one) in the span of 0.40 GPa. Meanwhile, the decrease of only 12 \AA^3 (1.5%) is noted for polymorph (IV), when pressure is increased from 0.50 to 0.78 GPa. The difference in susceptibility of crystals to compression is also reflected in the unit-cell volume compressibility (β_V). Initially, β_V is more than twice as high for polymorph (I) than for (IV). However, polymorph (I) crystals lose their softness with increasing pressure, as showed by the decrease in β_V value, but up to 0.41 GPa, they remain softer than crystals of polymorph (IV) [$\beta_V = 0.70 \text{ GPa}^{-1}$ for polymorph (I) at 0.41 GPa, compared to $\beta_V = 0.55 \text{ GPa}^{-1}$ for polymorph (IV) at 0.50 GPa]. It can be expected that on compression of polymorph (I) crystals above 0.41 GPa its compressibility β_V will decrease further, eventually becoming lower than for polymorph (IV). The decrease of β_V reflects the inability of molecular packing to adapt, resulting in increased structural strain. This, in turn, moves crystallization preference toward the new high-pressure polymorph (IV), of compressibility β_V hardly affected by the pressure in the range of 0.50–0.78 GPa [Fig. 1(a)]. Although compression of crystals of polymorph (I) to 0.60 GPa increases the strain, no phase transition was observed, and crystallization of polymorph (IV) was initiated instead. Similar cases, where polymorph formation required recrystallization, were described previously. Polymorphs formed during *in situ* high-pressure recrystallization that cannot be obtained as a result of solid-state phase transition were even termed *hidden*, as they can be easily missed when only the compression of sample crystals is performed (Paliwoda, 2012; Anioła & Katrusiak, 2015; Sobczak & Katrusiak, 2017).

Interestingly, crystals of both polymorphs, (I) and (IV), were found to compress anisotropically, with initial linear compressibility higher for directions [b] and [c] than for [a] (β_b , β_c and β_a , respectively). For polymorph (I), parameters β_b and β_c decrease with pressure, similarly to β_V , while β_a increases. As a result direction [a] becomes softer than [b] above 0.28 GPa, and equates with [c] at 0.41 GPa. Meanwhile, in polymorph (IV), linear compressibility of crystal in directions [a], [b] and [c] is affected in a lesser way, with an only slight decrease of β_b , and an increase of β_a and β_c observed in 0.50–0.78 pressure range.

The preference for the compression in [010] and [001] directions can be correlated with molecular aggregation in BZC crystals. It is worth noting that the primary aggregation motif of BZC molecules (N–H...O bonded ribbon) is common for all four polymorphs. For polymorphs (I)–(III) ribbons are positioned in a similar way (Fig. 2), all propagating parallel and antiparallel to the [100] direction. Only polymorph (IV) exhibits different positioning of ribbons in respect to each other, with every two parallel ribbons fitted on side of ethylene residue in a chainsaw mode, and then inclined in respect to the next adjacent ribbons at *ca* 80°. Therefore, two directions of parallel and antiparallel propagation can be distinguished: $[\bar{1}10]$ and $[1\bar{1}0]$.

In polymorph (I), hydrogen-bonded ribbons are either stacked or create a herringbone arrangement in the direction

[010] and are stacked or positioned in a zigzag mode in the direction [001] (Fig. 2). It leaves a void space between ribbons that can be gradually eliminated when pressure is increased, making the crystal initially softer in [010] and [001] directions. However, as the volume of the voids is reduced and hydrogen-bonded ribbons are forced to become closer, steric hindrance and repulsive interactions become more meaningful,

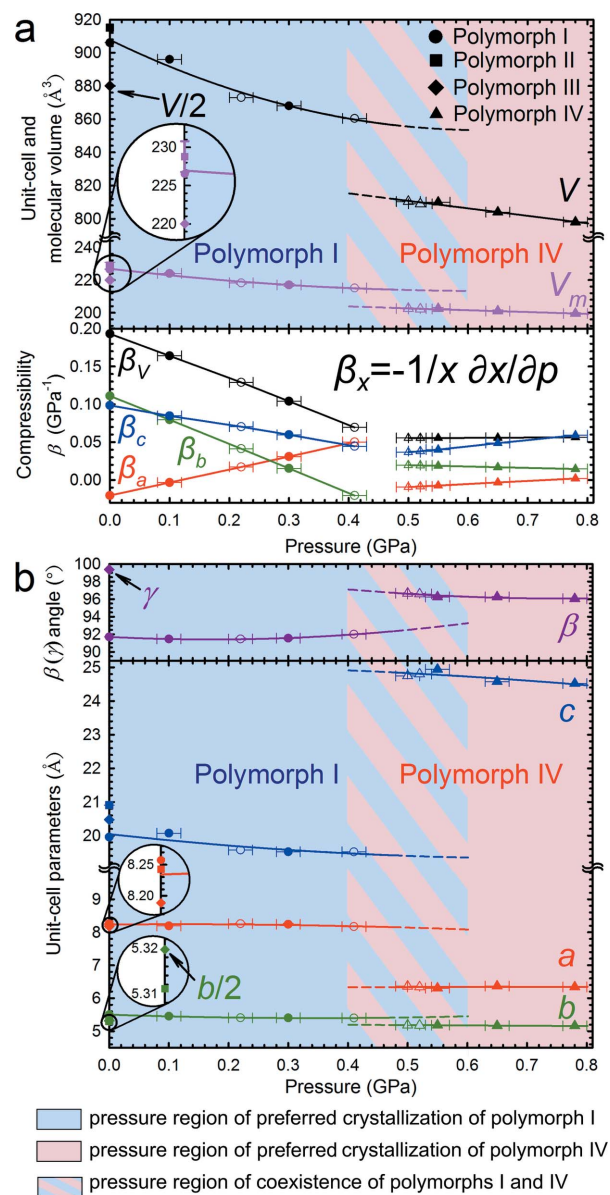


Figure 1

The pressure dependence of (a) unit-cell volume, molecular volume, and compressibility, as well as, (b) unit-cell parameters for BZC polymorphs (I) and (IV) (triangles). Unit-cell parameters for BZC polymorphs (II) (at 300 K, squares) and (III) (at 150 K, diamonds) have been included for comparison. Unit-cell volume and parameter b for polymorph (III) have been divided by two. High-pressure data collected for sample in MeOH:EtOH:H₂O 16:3:1 volume hydrostatic medium is marked with full symbols, while open symbols mark data collected with the use of DMSO as a hydrostatic medium. Trend lines were extended beyond data points as dashed lines to mark pressure regions where the form of BZC crystals was preserved on compression [polymorph (I)] or decompression [polymorph (IV)].

hindering further compression. Meanwhile, the ribbon propagation direction coincides with direction [100]. Due to the molecules in the ribbon being already close to each other, as a result of short hydrogen bonds formation, [100] is initially the hardest direction in the crystal. Nevertheless, the approach of the molecules within ribbons coincides with favourable shortening of hydrogen bonds, hence increase of the linear compressibility in [100] direction can be observed.

In polymorph (IV), the directions of ribbons propagation are interdependent with directions [100] and [010]. Because the linear compression along the ribbon axis is limited (due to the proximity of BZC molecules within ribbons), linear compression of crystals of polymorph (IV) in directions [100] and [010] is restricted, making direction [001] the softest. However, the inclined orientation of ribbons provides more compact packing compared to polymorphs (I)–(III). Therefore, a smaller void space that can be clenched on pressure increase is available. As a result, crystals of polymorph (IV) show lower compressibility in respect to polymorph (I).

The supramolecular heterosynthon (primary amine...ester synthon) formed in crystals of BZC coincide with the preference shown in crystal structures of compounds structurally similar to it reported so far. The CSD survey revealed that such synthon is formed in >96% of structures in the absence of other oxygen or nitrogen atoms. The investigated group contains 60 depositions. In 51, moieties are connected by $\text{NH}\cdots\text{O}=\text{C}$ contacts, in four by $\text{NH}\cdots\text{O}-\text{C}$, and in three structures both types of contacts are observed.

Similar to BZC, its analogous compounds show the tendency to form $\text{N}-\text{H}\cdots\text{O}$ contacts between primary amine and carboxyl atom of ester group leading to the creation of ribbon motif. In fact, this is the most common motif (60%) in crystal structures of esters of 4-aminobenzoic acid and its derivatives reported so far (including all BZC polymorphs). Further analysis showed that ribbons can be distinguished into

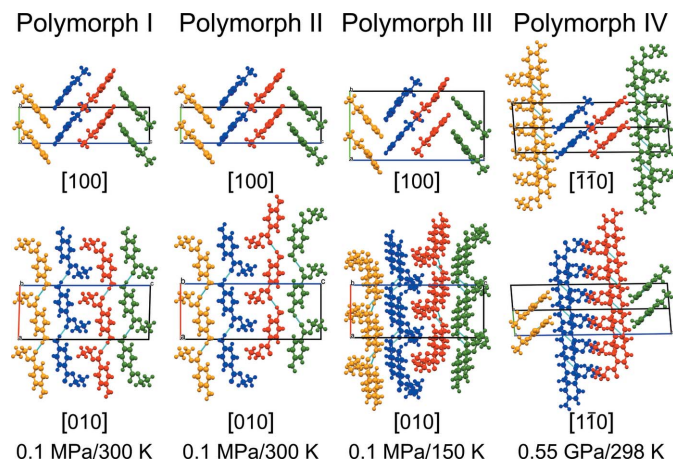


Figure 2

Molecular packing for four benzocaine polymorphs shown along with selected crystallographic directions. The ribbons are distinguished by different colours. Packing for polymorphs (I)–(III) are shown for previously reported structures (Chan *et al.*, 2009): QQQAXG04 [polymorph (I)], QQQAXG05 [polymorph (II)] and QQQAXG03 [polymorph (III)].

three variations (Fig. S15). Most commonly molecules arrange in the flat [BZC polymorphs (I)–(IV)] or step-like [polymorph (III)] way. However, if substituents are present in the *meta* position of the aromatic ring of the benzoic acid, ribbons can become twisted due to the steric and/or electrostatic effects

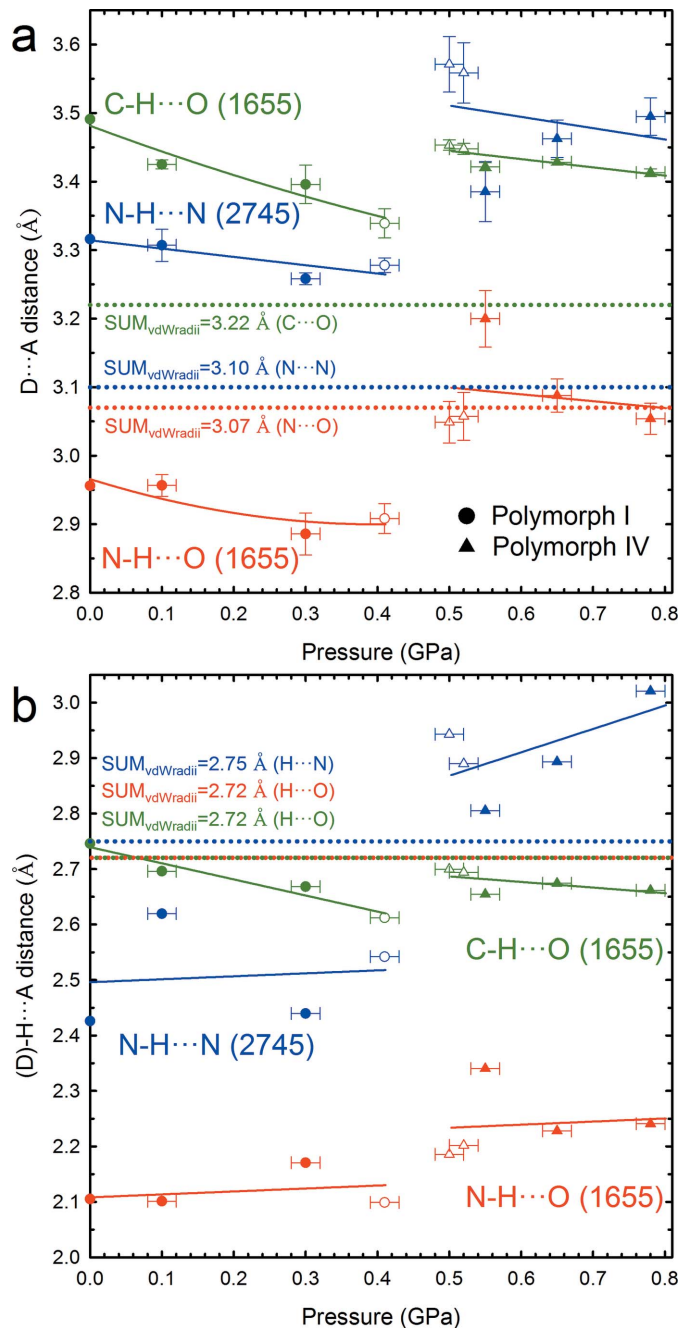


Figure 3

The pressure dependence of: (a) $\text{D}\cdots\text{A}$ and (b) $\text{H}\cdots\text{A}$ distances for $\text{N}-\text{H}\cdots\text{O}$, $\text{N}-\text{H}\cdots\text{N}$ and $\text{C}-\text{H}\cdots\text{O}$ contacts in crystals of BZC polymorphs (I) (circles) and (IV) (triangles), shown in red, blue and green, respectively. The sums of van der Waals radii are shown with dotted lines in corresponding colours. Data for samples obtained from $\text{MeOH}:\text{EtOH}:\text{H}_2\text{O}$ 16:3:1 volume solution are marked with full symbols, while open symbols mark data collected using DMSO. The *ORTEP* symmetry codes (Farrugia, 2012) are explained in Table S2. Data points at 0.1 MPa were calculated based on the previously reported structure, refcode QQQAXG04 (Chan *et al.*, 2009).

(e.g. BIZFIA, HOCJAM; Xie *et al.*, 2014). Moreover, in most of the deposited structures, including BZC polymorphs (I)–(III), there is a tendency for ribbons to propagate in only one direction. Although the ribbon is the most common motif, there are seven deposits exemplifying alternative N–H···O bonded molecular arrangement: (i) five where molecules are forming tetramers; (ii) one exemplifying 2D net; (iii) one with zig-zag chain motif (Fig. S15). Intriguingly, methyl 4-aminobenzoate, structurally very close to BZC, is so far the only ester of 4-aminobenzoic acid with two solid forms reported, each one exemplifying different aggregation motif: ribbon (CEBGUL01) and tetramer (CEBGUL; Lin, 1983), both shown in Fig. S15. It is surprising that despite the molecular similarity of BZC, the tetramer motif occurred in none of its known polymorphs.

Due to the way molecules are oriented to form the of N–H···O hydrogen bonds, the ribbon motif can be additionally supported by C–H···O contacts, formed by an aromatic hydrogen atom (in *ortho* position in respect to the amine group) and carbonyl of the adjacent BZC molecule. However, despite adequate molecular orientation, in case of polymorphs (I) and (II), aromatic hydrogen atoms and carbonyl groups of neighbouring molecules are too far apart, and no such contact can be distinguished. Only when crystals of polymorph (I) are compressed in the DAC, molecules approach each other and the distance between hydrogen and oxygen atoms decrease leading to the formation of the

C–H···O contact (Figs. 3 and S16, and Table S3). Such hydrogen-bond is also present in polymorphs (III) and (IV), but its formation can be explained in terms of thermal contraction [polymorph (III)] or compression [polymorph (IV)]. Interestingly, in polymorph (IV), the geometry of both, N–H···O hydrogen bond and C–H···O contact, becomes less favourable, as showed by them becoming longer than in polymorph (I) at the pressure of 0.41 GPa (Fig. 3).

Alongside N–H···O hydrogen bonds, and occasional C–H···O contacts connecting BZC molecules into ribbons, we can distinguish additional contacts between ribbons. The major cohesion force connecting ribbons in polymorphs (I)–(III) are N–H···N hydrogen bonds, additionally supported by C–H··· π interactions. The reorientation of ribbons in polymorph (IV) prevents the formation of any N–H···N contacts (Figs. 3, 4 and S16, and Table S3), making weak C–H··· π interactions the major cohesion force bonding BZC ribbons together (Fig. S17 and Table S4).

The distortion of the hydrogen-bonding pattern in polymorph (IV) can be observed in the comparison of Full Interaction Maps (FIMs; Wood *et al.*, 2013). Polymorph (I) clearly fulfils the desired interactions to a higher extent than polymorph (IV), with all regions of preferred geometry for intermolecular contacts coinciding with the positioning of acceptor and donor groups of adjacent molecules (Fig. 5). However, in case of interacting amine groups, the primary amine donor and acceptor groups lay on the borderlines of the propensity regions. In polymorph (IV) only the regions within hydrogen-bonded ribbon are fulfilled, and two propensity regions in proximity of BZC amine group remain vacant, with amine groups of adjacent molecules visibly beyond them. Interestingly, the FIMs are used to investigate the propensity of a given compound to polymorphism based on the fulfilment of the interaction landscape in the known crystal forms (Wood *et al.*, 2013). Therefore, polymorphs exhibiting hydrogen-bonding pattern of more preferred geometry than that observed in the ambient-condition BZC polymorph (I), should be expected. Instead, crystallization in the form of the polymorph (IV) leads to weakening of the hydrogen bonds between hydrogen-bonded BZC ribbons, leaving interaction landscape unfulfilled.

The precise comparison of the significance of different types of contacts in supporting the crystal structure can be assessed from the overlap of their van der Waals radii. The overlap can be expressed as δ parameter:

$$\delta = r_{AB} - vdW_A - vdW_B, \quad (1)$$

where r_{AB} is the distance between atoms A and B, and vdW_A and vdW_B are their van der Waals radii (Kaźmierczak & Katrusiak, 2013, 2014, 2015).

When all contacts in crystal structures of BZC polymorphs (I) and (IV) are analysed in terms of their δ parameter, N–H···O hydrogen bond is the contact with the smallest δ value in both cases, even despite it becoming slightly longer in polymorph (IV) (Fig. 6). This is in agreement with the previously reported analysis of the shortest contacts hierarchy in crystals of compounds manifesting high-pressure poly-

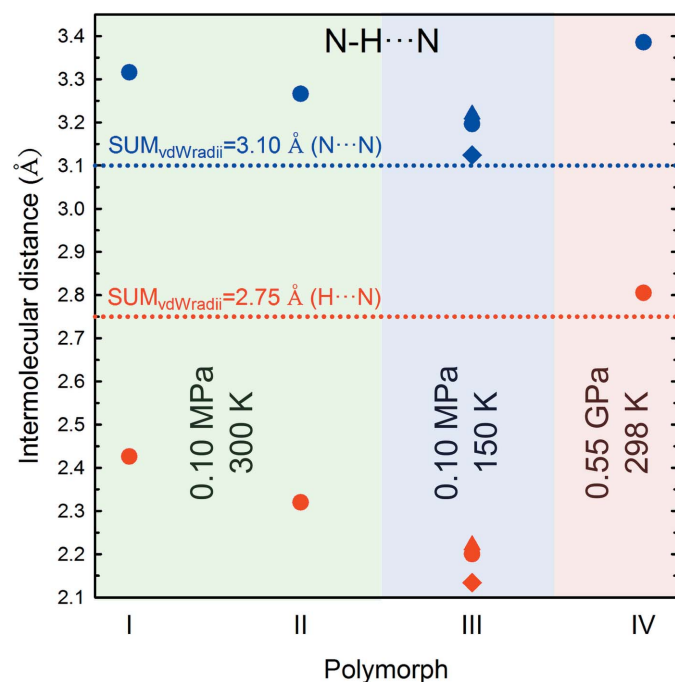


Figure 4 Intermolecular distance between nitrogen–nitrogen (blue) and hydrogen–nitrogen (red) atoms in N–H···N hydrogen bonds in all four BZC polymorphs. The sums of van der Waals radii are shown with dotted lines in corresponding colours. Due to the $Z' = 4$ for polymorph (III), values for three symmetry-independent N–H···N hydrogen bonds were included. Distances for polymorphs (I)–(III) are shown for previously reported structures (Chan *et al.*, 2009): QQQAXG04 [polymorph (I)], QQQAXG05 [polymorph (II)] and QQQAXG03 [polymorph (III)].

morphism, showing that the nature of the shortest contact, relative to the sum of van der Waals radii, remains unchanged (Kaźmierczak & Katrusiak, 2015). At the same time, a significant rearrangement in contacts of larger δ value can be observed (Kaźmierczak & Katrusiak, 2015; Marciniak *et al.*, 2016a), and such tendency is present in BZC (Fig. 6). Notably, the N–H...N hydrogen bond is the contact with the second smallest δ value in BZC polymorph (I) up to 0.41 GPa, while in polymorph (IV) it is not even the tenth contacts with the smallest δ value.

Besides the more favourable hydrogen-bonding pattern, the enthalpy of formation also gives an indication that BZC polymorph (I) is thermodynamically more stable than polymorph (IV) (Fig. 7), with the energy calculated for unit cells of

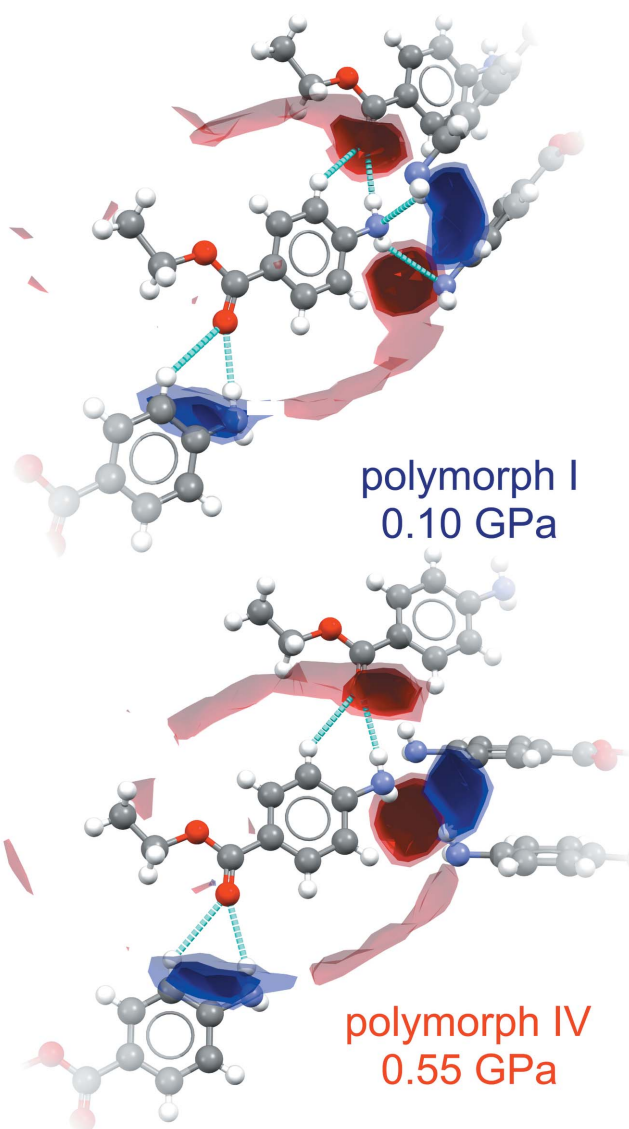


Figure 5
Full interaction maps (FIMs) calculated with programme *Mercury* (Bruno *et al.*, 2002; Wood *et al.*, 2013) for BZC polymorphs (I) and (IV) at 0.10 and 0.55 GPa, respectively. The propensity regions of preferred geometry for the position of carbonyl H-acceptors and amine H-donors/acceptors are shown in red and blue, respectively. Hydrogen bonds are shown in cyan.

each form differing of about -15 kJ mol^{-1} . Such difference might originate from the reduction and attenuation of contacts supporting crystal structure, especially the elimination of N–H...N hydrogen bonds. In these terms, it would appear that preference for crystallization of BZC polymorph (IV) is kinetically driven, and can be associated with achieving more dense packing under high pressure.

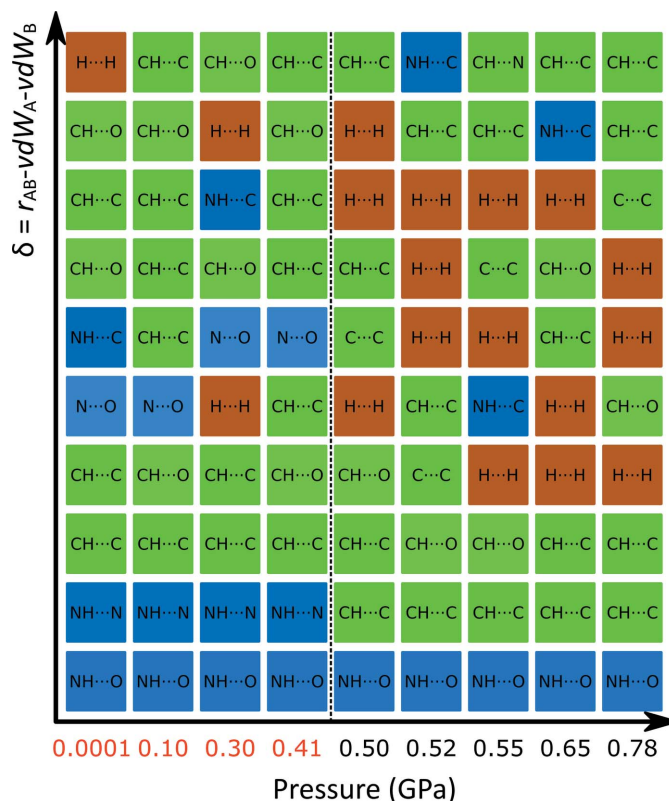


Figure 6
The short contacts sorted by increasing value of δ parameter in the function of pressure. The dotted line divides polymorphs (I) and (IV). Analysis of ambient-condition structure was performed using previously reported data (CSD refcode: QQQAXG09; Patel *et al.*, 2017). Where required, the positions of hydrogen atoms were normalized to C–H = 1.083 Å, N–H = 1.009 Å (Groom *et al.*, 2016).

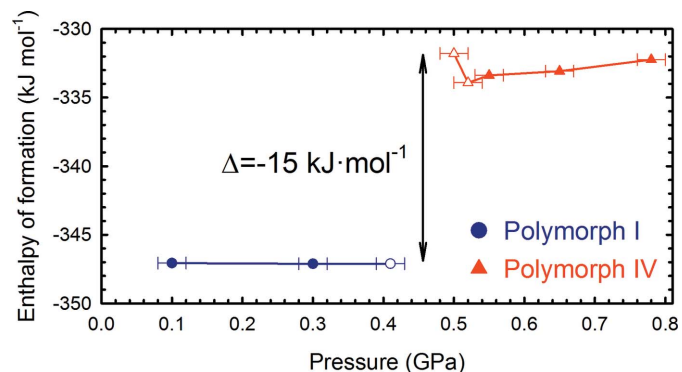


Figure 7
Enthalpy of formation of high-pressure structures of polymorphs (I) (blue) and (IV) (red). Data for samples obtained from MeOH:EtOH:H₂O 16:3:1 volume solution are marked with full symbols, while open symbols mark data collected with the use of DMSO.

4. Conclusions

A new, high-pressure benzocaine polymorph (IV) has been discovered above 0.45 GPa, and it can be obtained either by isochoric or isothermal crystallization. The molecules of BZC in polymorph (IV) form N—H...O bonded ribbons similar to those found in the polymorphs (I)–(III). It shows that even increased pressure was not able to enforce a change of the major aggregation motif of BZC molecules. Nevertheless, the respective orientation of ribbons in the newly obtained crystal form was altered: hydrogen-bonded ribbons propagate parallel and antiparallel to only one direction, [100], in polymorphs (I)–(III), and to two distinctive directions, $[1\bar{1}0]$ and $[\bar{1}10]$, in polymorph (IV). Despite the fact that the shortest contact, *i.e.* N—H...O hydrogen bond, is preserved above 0.45 GPa, a significant change in the hierarchy of longer contacts can be observed. The most prominent change concerns N—H...N hydrogen bonds. Those bonds are the major cohesion force connecting ribbons in polymorphs (I)–(III), but they are eliminated in high-pressure polymorph (IV). Impairment of the hydrogen-bonding pattern is reflected in enthalpy of formation, that is about 15 kJ mol⁻¹ higher for polymorph (IV) than for polymorph (I), indicating its lower thermodynamic stability. This suggests that crystallization of polymorph (IV) is kinetically driven and it can be associated with achieving more dense packing under high pressure. Unfortunately, crystals of polymorph (IV) are not preserved on pressure release. On rapid decompression to ambient pressure, transformation to polymorph (II) occurs. However, if the sample remains in DAC after pressure decreases below 0.2 GPa, over the time BZC recrystallizes in the form of polymorph (I).

5. Related literature

References cited in the supporting information include: Arunan *et al.* (2011), Brandl *et al.* (2001), Katrusiak (2003).

Acknowledgements

We are grateful to Professor Andrzej Katrusiak, Dr Marcin Podsiadło and Dr Anna Olejniczak from Faculty of Chemistry, Adam Mickiewicz University in Poznań for useful discussions. We would also like to thank Dr Joanna Gościańska from Faculty of Chemistry, Adam Mickiewicz University in Poznań for supplying the sample of benzocaine.

References

Aguado, E., León, I., Millán, J., Cocinero, E. J., Jaeqx, S., Rijs, A. M., Lesarri, A. & Fernández, J. A. (2013). *J. Phys. Chem. B*, **117**, 13472–13480.
 Amidon, G. L., Lennernäs, H., Shah, V. P. & Crison, J. R. (1995). *Pharm. Res.* **12**, 413–420.
 Anioła, M. & Katrusiak, A. (2015). *Cryst. Growth Des.* **15**, 764–770.
 Arunan, E., Desiraju, G. R., Klein, R. A., Sadlej, J., Scheiner, S., Alkorta, I., Clary, D. C., Crabtree, R. H., Dannenberg, J. J., Hobza, P., Kjaergaard, H. G., Legon, A. C., Mennucci, B. & Nesbitt, D. J. (2011). *Pure Appl. Chem.* **83**, 1637–1641.

Bis, J. A., Vishweshwar, P., Weyna, D. & Zaworotko, M. J. (2007). *Mol. Pharm.* **4**, 401–416.
 Boldyreva, E. (2007). *Cryst. Growth Des.* **7**, 1662–1668.
 Boldyreva, E. (2016). *Curr. Pharm. Des.* **22**, 4981–5000.
 Bondi, A. (1964). *J. Phys. Chem.* **68**, 441–451.
 Bottari, F., Di Colo, G., Nannipieri, E., Saettoni, M. F. & Serafini, M. F. (1977). *J. Pharm. Sci.* **66**, 926–931.
 Braga, D., Grepioni, F., Maini, L. & Polito, M. (2009). *Molecular Networks*, edited by M. W. Hosseini, pp. 87–95. Berlin, Heidelberg: Springer.
 Brandl, M., Weiss, M. S., Jabs, A., Sühnel, J. & Hilgenfeld, R. (2001). *J. Mol. Biol.* **307**, 357–377.
 Bruno, I. J., Cole, J. C., Edgington, P. R., Kessler, M., Macrae, C. F., McCabe, P., Pearson, J. & Taylor, R. (2002). *Acta Cryst.* **B58**, 389–397.
 Bučar, D.-K., Henry, R. F., Zhang, G. G. Z. & MacGillivray, L. R. (2014). *Cryst. Growth Des.* **14**, 5318–5328.
 Butterworth, J. F. & Strichartz, G. R. (1990). *Anesthesiology*, **72**, 711–734.
 Chan, E. J., Rae, A. D. & Welberry, T. R. (2009). *Acta Cryst.* **B65**, 509–515.
 Cheney, M. L., Weyna, D. R., Shan, N., Hanna, M., Wojtas, L. & Zaworotko, M. J. (2010). *Cryst. Growth Des.* **10**, 4401–4413.
 Rigaku Oxford Diffraction (2015). *CrysAlis PRO*. Rigaku Oxford Diffraction, Yarnton, England.
 Fabbiani, F. P. A., Allan, D. R., David, W. I. F., Davidson, A. J., Lennie, A. R., Parsons, S., Pulham, C. R. & Warren, J. E. (2007). *Cryst. Growth Des.* **7**, 1115–1124.
 Fabbiani, F. P. A., Allan, D. R., David, W. I. F., Moggach, S. A., Parsons, S. & Pulham, C. R. (2004). *CrystEngComm*, **6**, 505–511.
 Fabbiani, F. P. A. & Pulham, C. R. (2006). *Chem. Soc. Rev.* **35**, 932–942.
 Farrugia, L. J. (2012). *J. Appl. Cryst.* **45**, 849–854.
 FDA (2007). ANDAs: Pharmaceutical Solid Polymorphism Chemistry, Manufacturing, and Controls Information. Rockville, MD: US Department of Health and Human Services Food and Drug Administration. Center for Drug Evaluation and Research.
 Gadade, D. D. & Pekamwar, S. S. (2016). *Adv. Pharm. Bull.* **6**, 479–494.
 Gao, Y., Gesenberg, C. & Zheng, W. (2017). *Developing Solid Oral Dosage Forms*, 2nd ed., edited by Y. Qiu, Y. Chen, G. G. Z. Zhang, L. Yu & R. V. Mantri, pp. 455–495. Boston: Academic Press.
 Geng, N., Chen, J.-M., Li, Z.-J., Jiang, L. & Lu, T.-B. (2013). *Cryst. Growth Des.* **13**, 3546–3553.
 Groom, C. R., Bruno, I. J., Lightfoot, M. P. & Ward, S. C. (2016). *Acta Cryst.* **B72**, 171–179.
 Hanck, D. A., Nikitina, E., McNulty, M. M., Fozzard, H. A., Lipkind, G. M. & Sheets, M. F. (2009). *Circ. Res.* **105**, 492–499.
 Johnstone, R. D. L., Lennie, A. R., Parker, S. F., Parsons, S., Pidcock, E., Richardson, P. R., Warren, J. E. & Wood, P. A. (2010). *CrystEngComm*, **12**, 1065–1078.
 Juni, K., Nakano, M. & Arita, T. (1977). *Chem. Pharm. Bull.* **25**, 1098–1100.
 Katrusiak, A. (2003). *Crystallogr. Rev.* **9**, 91–133.
 Kaźmierczak, M. & Katrusiak, A. (2013). *J. Phys. Chem. C*, **117**, 1441–1446.
 Kaźmierczak, M. & Katrusiak, A. (2014). *Cryst. Growth Des.* **14**, 2223–2229.
 Kaźmierczak, M. & Katrusiak, A. (2015). *CrystEngComm*, **17**, 9423–9430.
 Law, V., Knox, C., Djoumbou, Y., Jewison, T., Guo, A. C., Liu, Y., Maciejewski, A., Arndt, D., Wilson, M., Neveu, V., Tang, A., Gabriel, G., Ly, C., Adamjee, S., Dame, Z. T., Han, B., Zhou, Y. & Wishart, D. S. (2014). *Nucleic Acids Res.* **42**, D1091–D1097.
 Lee, E. H. (2014). *Asia. J. Pharm. Sci.* **9**, 163–175.
 Lin, X. (1983). *Jiegou Huaxue*, pp. 219–221.
 Lynch, D. E. & McClenaghan, I. (2002). *Acta Cryst.* **E58**, o708–o709.

- Marciniak, J., Bąkiewicz, J., Dobrowolski, M. A., Dziubek, K. F., Kaźmierczak, M., Paliwoda, D., Rajewski, K. W., Sobczak, S., Stachowicz, M. & Katrusiak, A. (2016a). *Cryst. Growth Des.* **16**, 1435–1441.
- Marciniak, J., Kaźmierczak, M., Rajewski, K. W. & Katrusiak, A. (2016b). *Cryst. Growth Des.* **16**, 3917–3923.
- Mehta, M. (2017). *Biopharmaceutics Classification System (BCS): Development, Implementation, and Growth*. Wiley-Blackwell.
- Merrill, L. & Bassett, W. A. (1974). *Rev. Sci. Instrum.* **45**, 290–294.
- Neumann, M. A., van de Streek, J., Fabbiani, F. P. A., Hidber, P. & Grassmann, O. (2015). *Nat. Commun.* **6**, 7793.
- Paczkowska, M., Wiergowska, G., Miklaszewski, A., Krause, A., Mroczkowska, M., Zalewski, P. & Cielecka-Piontek, J. (2018). *Molecules*, **23**, 1737.
- Paliwoda, D. K., Dziubek, K. F. & Katrusiak, A. (2012). *Cryst. Growth Des.* **12**, 4302–4305.
- Patel, M. A., AbouGhaly, M. H. H. & Chadwick, K. (2017). *Int. J. Pharm.* **532**, 166–176.
- Patyk, E., Jenczak, A. & Katrusiak, A. (2016). *Phys. Chem. Chem. Phys.* **18**, 11474–11479.
- Patyk, E. & Katrusiak, A. (2015). *Chem. Sci.* **6**, 1991–1995.
- Patyk, E., Podsiadło, M. & Katrusiak, A. (2015a). *Cryst. Growth Des.* **15**, 4039–4044.
- Patyk, E., Podsiadło, M. & Katrusiak, A. (2015b). *Cryst. Growth Des.* **15**, 5670–5674.
- Patyk, E., Skumiel, J., Podsiadło, M. & Katrusiak, A. (2012). *Angew. Chem. Int. Ed.* **51**, 2146–2150.
- Piermarini, G. J., Block, S., Barnett, J. D. & Forman, R. A. (1975). *J. Appl. Phys.* **46**, 2774–2780.
- Shattock, T. R., Arora, K. K., Vishweshwar, P. & Zaworotko, M. J. (2008). *Cryst. Growth Des.* **8**, 4533–4545.
- Sheldrick, G. M. (2015a). *Acta Cryst.* **A71**, 3–8.
- Sheldrick, G. M. (2015b). *Acta Cryst.* **C71**, 3–8.
- Sinha, B. K. & Pattabhi, V. (1987). *Proc. Indian Acad. Sci. Chem. Sci.* **98**, 229–234.
- Smith, A. J., Kavuru, P., Wojtas, L., Zaworotko, M. J. & Shytle, R. D. (2011). *Mol. Pharm.* **8**, 1867–1876.
- Sobczak, S. & Katrusiak, A. (2017). *J. Phys. Chem. C*, **121**, 2539–2545.
- Stewart, J. J. P. (2016). *MOPAC2016*. <http://openmopac.net>.
- Wood, P. A., Olsson, T. S. G., Cole, J. C., Cottrell, S. J., Feeder, N., Galek, P. T. A., Groom, C. R. & Pidcock, E. (2013). *CrystEngComm*, **15**, 65–72.
- Xie, J., Yuan, X., Abdukader, A., Zhu, C. & Ma, J. (2014). *Org. Lett.* **16**, 1768–1771.
- Zakharov, B. A. & Boldyreva, E. V. (2019). *CrystEngComm*, **21**, 10–22.
- Zakharov, B. A., Seryotkin, Y. V., Tumanov, N. A., Paliwoda, D., Hanfland, M., Kurnosov, A. V. & Boldyreva, E. V. (2016). *RSC Adv.* **6**, 92629–92637.